Micro-Ring Modulator Linearity Enhancement for Analog and Digital Optical Links

Sumilak Chaudhury, Karl Johnson, Vladimir Fedorov, Bill Lin, *Member, IEEE*, Yeshaiahu Fainman, *Life Fellow, IEEE*, and Tzu-Chien Hsueh, *Senior Member, IEEE*

***Abstract*—An energy/area-efficient low-cost broadband linearity enhancement technique using the hybrid of notch-filter and bandpass-filter micro-ring modulators (Hybrid-MRMs) is proposed to achieve higher than 3.01-dB improvement in spurious-free-dynamic-ranges with intermodulation distortions ($\Delta SFDR_{IMD}$) and 17.9-dB improvement in integral nonlinearity (ΔINL_{PP}) over a conventional notch-filter MRM (NF-MRM) across a 4.8-dB extinction-ratio full-scale range based on rapid silicon-photonics fabrication results for the emerging applications of various analog and digital optical communication systems.**

***Index Terms*—Analog optical link, electro-optic modulator, integral nonlinearity, intensity modulation, microresonator, micro-ring modulator, radio-frequency photonics, RF-over-fiber.**

I. Introduction

ANALOG optical communication systems have become increasingly important in the emerging applications of radio-frequency (RF) photonic links [1], radio-over-fiber, subcarrier transmissions, and phased array antennae [2]. The nonlinearity of electro-optic modulators used in analog electrical-to-optical (E/O) interfaces induces RF signal distortions, limits dynamic ranges, and dominates overall link performance. Many research projects have been focusing on mitigating the nonlinearity issues of Mach-Zehnder modulators (MZM) covering from high-linearity Lithium Niobate ($LiNbO_3$) discrete MZMs [3] to heterogeneously integrated III-V/silicon MZMs [4], [5]. However, even in the most advanced monolithic silicon-photonics (M-SiPh) process technology at GlobalFoundries (GF45SPCLO) [6], the on-chip area of an MZM is still in the range of multiple mm^2. As such, analog amplifiers or digital drivers interfacing with MZMs have to treat the MZM electrodes as transmission lines (TL) with the design effort of characteristic impedance matching network and the power/area overhead of on-chip terminations [7] when the RF signal frequencies or Nyquist frequencies of optical links are close to or higher than 10 GHz, which renders sub-optimal energy/area efficiency and further induces power density violations as well as device reliability issues.

Received 18 July 2024; revised 26 October 2024; accepted 28 October 2024. Date of publication 31 October 2024; date of current version 6 November 2024. This work was supported in part by the National Science Foundation under Award 2023730, Award 2025752, Award 2045935, Award 2217453, and Award 2410053; and in part by ASML/Cymer Corporation. *(Corresponding author: Tzu-Chien Hsueh.)*

The authors are with the Department of Electrical and Computer Engineering, University of California, San Diego, La Jolla, CA 92093 USA (e-mail: tzhsueh@ucsd.edu).

Color versions of one or more figures in this letter are available at https://doi.org/10.1109/LPT.2024.3488699.

Digital Object Identifier 10.1109/LPT.2024.3488699

Notch-filter micro-ring modulators (NF-MRM) have been widely used in high-speed pulse-amplitude modulation (PAM) digital data communication systems [8] because their compact silicon areas and footprints, which can be more than 800× smaller than an MZM in GF45SPCLO, tremendously reduce the electrical signal traveling distances between the amplifier/driver outputs and MRM electrodes. In other words, an MRM-based E/O interface can be treated as lumped and small capacitive circuitry to enable twofold improvements in energy, area, and integration efficiencies. However, using optical power intensity modulation (IM) through the NF-MRM [9] inevitably produces a very nonlinear E/O-conversion transfer function even within a small extinction-ratio (ER) full-scale (FS) range. Multiple MRM linearity enhancement techniques have been proposed; however, the segmented MRM in [10] is only sufficient for high-speed low-resolution (i.e., 2 bit/symbol or PAM-4) digital optical links; the MRM quality-factor manipulation in [11] requires specific coupling gaps sensitive to process, voltage, temperature (PVT) variations; the hybrid silicon-and-$LiNbO_3$ MRM in [12] is not effectively compatible with commercial CMOS process technology.

To retain the excellent energy/area benefits of an MRM and extend its applications to both analog and digital optical links without sophisticated linearization techniques [11], [12], this letter proposes a low-cost linearity enhancement technique using the hybrid of notch-filter and bandpass-filter MRMs (Hybrid-MRMs) to achieve higher than 3.01-dB dynamic-linearity improvement in spurious-free-dynamic-ranges with intermodulation distortions ($\Delta SFDR_{IMD}$) and 17.9-dB static-linearity improvement in peak-to-peak integral nonlinearity (ΔINL_{PP}) over the conventional NF-MRM across a 4.8-dB ER FS range. Note that there are two versions of the proposed Hybrid-MRM transmitter (TX) shown in Fig. 1. For the sake of simplicity, the technical analyses, simulations, and experimental validations in Sections II and III focus on the architecture in Fig. 1(a), and the other in Fig. 1(b) is discussed in Section IV.

II. MRM Linearity Enhancement Technique

The linearity enhancement technique illustrated in Fig. 1(a) is established on top of the NF-MRM with the circuit configuration shown in the upper half of Fig. 1(a), whose E/O conversion can be represented by the signal processing flow from the electrical signal V_P driven by the linear amplifier to the NF-MRM Through-Port output optical power P_{thru}; note that P_{in} (= P_λ) is a constant laser power with a wavelength of λ

injected into the NF-MRM Input-Port, not the electrical signal power at V_P. According to certain design specifications of an E/O interface and integrated photonics process technology, the free spectral range (FSR), radius, coupling coefficient, quality factor (Q), optical frequency band, and initial resonant frequency of the NF-MRM can be properly determined, and then, by influencing the refractive-index magnitude of the NF-MRM resonant cavity during signal transmissions, the static-control knob of shifting the power response w.r.t the wavelength axis is the thermal control (or heater) voltage $V_{heat,NF}$ while the dynamic-control knob of shifting the power response w.r.t the wavelength axis is the reverse bias $(V_N - V_P)$ of the segmented PN junctions underneath the ring waveguide of the NF-MRM. As the normalized power response P_{thru}/P_{in} shown in Fig. 2(a), the default spectrum and notch point of P_{thru}/P_{in} can be designated by $V_{heat,NF}$ as the green curve when V_P is set to its minimum ($V_{P,min}$), and in principle, the whole P_{thru}/P_{in} response can be shifted to the position of the light-green curve when V_P is set to its maximum ($V_{P,max}$). Therefore, if V_P is continuously varying between $V_{P,min}$ and $V_{P,max}$, i.e., electrical signal FS, like the black sinusoid waveform in Fig. 2(a), then the optical power P_{thru} at the NF-MRM Through-Port shall vary accordingly within the output FS like the red sinusoid waveform in Fig. 2(a) as well, which is the essential concept of the IM-based E/O conversion through the NF-MRM. Note that since V_N is a constant voltage from a low-impedance voltage supply, the electrical bandwidth dominating the whole E/O interface is determined by the linear amplifier output impedance and PN junction capacitance of the NF-MRM at V_P. Because of the compact footprint per MRM in general and advanced M-SiPh process technology [6], the electrical bandwidth at V_P can reasonably reach higher than 10 GHz without energy/area overhead due to TLs and impedance matching network.

The mechanism of the E/O conversion through the NF-MRM described in Fig. 2(a) has two major sources of nonlinearity: The first one is how linear or straight the P_{thru}/P_{in} response (green curve) can perform within the optical power FS (between the two horizontal dash lines), which can be quantified by the static-linearity metric, INL_{PP}, of the E/O-conversion transfer curves. The second one is how the P_{thru}/P_{in} response can be linearly shifted within the electrical signal FS (between the two vertical dash lines) under the effect of the PN-junction reverse bias influencing the Q and refractive-index magnitude, which can be all covered by the dynamic-linearity metric, $SFDR_{IMD}$, in the third intercept point (IP_3) measurements [9] with, for example, the precise MRM models in GF45SPCLO.

The proposed linearity enhancement is achieved by adding a bandpass-filter MRM (BF-MRM), which is also driven by the same reverse bias of the NF-MRM but has an independent thermal control voltage $V_{heat,BF}$ as shown in the lower half of Fig. 1(a). The fundamentals of the NF-MRM and BF-MRM are basically identical; their primary difference is that the input/output port configuration of the BF-MRM renders its E/O conversion to be the signal processing flow from the electrical signal V_P driven by the linear amplifier to the BF-MRM Drop-Port output optical power P_{drop}, which possesses

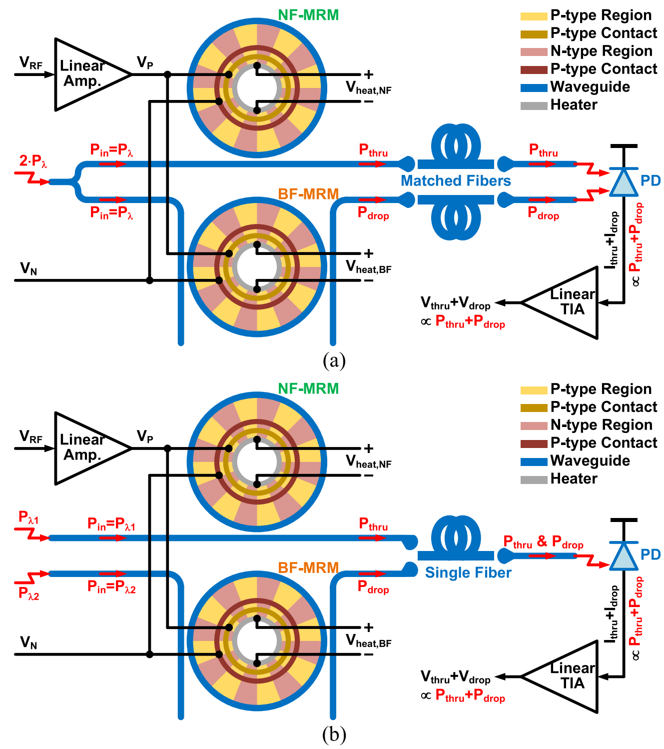

Fig. 1. The circuit schematic of the MRM linearity enhancement technique (Hybrid-MRMs: NF-MRM + BF-MRM) on top of the conventional NF-MRM with (a) a single laser wavelength and two matched fibers or (b) two laser wavelengths and a single fiber.

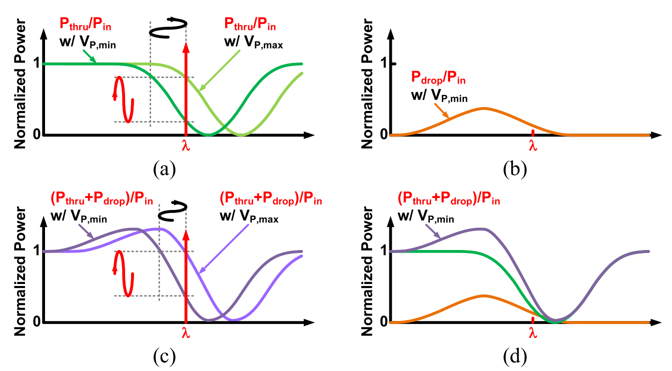

Fig. 2. The normalized power responses of (a) the NF-MRM with electrical signal V_P modulation, (b) the BF-MRM, (c) the Hybrid-MRMs with electrical signal V_P modulation, and (d) the Hybrid-MRMs achieved by summing the power responses of the NF-MRM and BF-MRM.

a peaking response (orange curve) as the normalized power response P_{drop}/P_{in} as shown in Fig. 2(b). Therefore, the key idea of this technique is to exploit the complementary power responses of the NF-MRM and BF-MRM to form the Hybrid-MRMs, as shown in the full picture of Fig. 1(a) for overall linearity enhancement, which contains multiple design parameters between the NF-MRM and BF-MRM for optimizing the degree of the linearity enhancement. The following technical description assumes that the NF-MRM and BF-MRM have unified ring radii, waveguide widths, coupling spacing, etc., specified by the standard-cell design library of GF45SPCLO, except $V_{heat,NF}$ and $V_{heat,BF}$ as the external control knobs can independently configure the resonant frequencies of the NF-MRM and BF-MRM to properly misalign the default notch

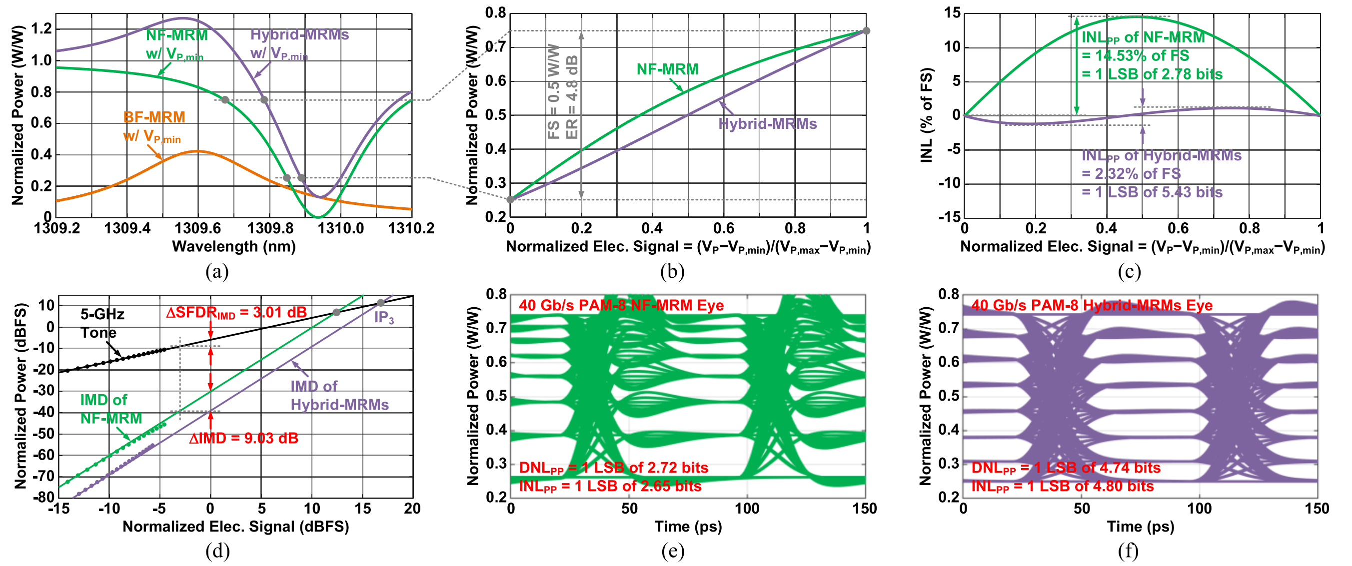

Fig. 3. The simulation results using O-band MRMs in GF45SPCLO: (a) The normalized power responses of the NF-MRM, BF-MRM, and Hybrid-MRMs when $V_P = V_{P,min}$. (b) The static E/O-conversion transfer curves of the NF-MRM and Hybrid-MRMs. (c) The INLs of the static E/O-conversion transfer curves in (b). (d) The IMDs in the IP_3 measurements of the NF-MRM and Hybrid-MRMs when V_P is a 5-GHz RF signal. (e) The time-domain eye-diagram of the NF-MRM when V_P is 40-Gb/s PAM-8 random data. (f) The time-domain eye-diagram of the Hybrid-MRMs when V_P is 40-Gb/s PAM-8 random data.

point and peaking point of P_{thru}/P_{in} (green curve) and P_{drop}/P_{in} (orange curve), respectively, as shown in Fig. 2(d) when V_P is set to $V_{P,min}$.

Under the settings described above, if these two power responses can be linearly and incoherently summed, the peaking spectrum of P_{drop}/P_{in} can be used to compensate for the flat and non-steep spectrum of the nonlinear P_{thru}/P_{in} region while the low power and almost zero spectrum of P_{drop}/P_{in} can negligibly affect the steep spectrum of the linear P_{thru}/P_{in} region. Equivalently, the normalized power response of the Hybrid-MRMs can be expressed as $(P_{thru} + P_{drop})/P_{in}$ illustrated by the purple curve in Fig. 2(d), whose linear region is pronouncedly larger than that of the P_{thru}/P_{in} response. Once the reverse biases of the NF-MRM and BF-MRM are simultaneously modulated by the electrical signal V_P like the black sinusoid waveform in Fig. 2(c), the P_{thru}/P_{in}, P_{drop}/P_{in}, and $(P_{thru} + P_{drop})/P_{in}$ responses can be all shifted together w.r.t the wavelength axis between the purple and light-purple curves. Because of the larger linear region and steeper slope of the $(P_{thru} + P_{drop})/P_{in}$ response, to reach the same amount of total optical power FS, the required electrical signal FS of the Hybrid-MRMs can be reduced accordingly. In other words, the Hybrid-MRM TX offers both higher E/O linearity and output optical power by taking advantage of the BF-MRM Drop-Port peaking spectrum and doubled laser injection power (i.e., $2{\cdot}P_{in}$) as shown in Fig. 2(d) and Fig. 1(a), respectively.

III. Simulations and Rapid Experiments

The Hybrid-MRM TX is simulated by using the O-band MRMs with less than 30-μm × 30-μm area per footprint in GF45SPCLO. As shown in Fig. 3(a), the Hybrid-MRM power response is constructed by the linear summation of the NF-MRM and BF-MRM power responses. By defining the normalized power FS range from 0.25 to 0.75, which is equivalent to a 4.8-dB ER, the static E/O-conversion transfer curves of the NF-MRM and Hybrid-MRMs w.r.t their

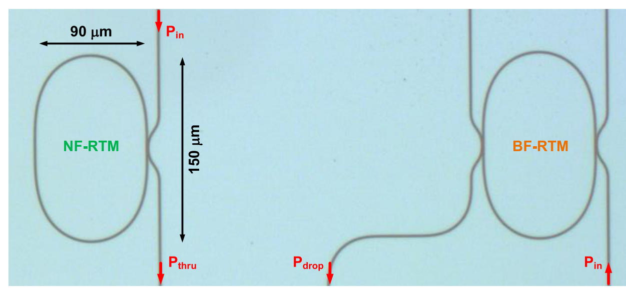

Fig. 4. The chip photo of the passive RTM linearity enhancement technique (Hybrid-RTMs: NF-RTM + BF-RTM) for rapid experimental validations.

normalized electrical signals at V_P are shown in Fig. 3(b), where the Hybrid-MRM transfer curve is much close to a straight line than the NF-MRM transfer curve. Their deviations from the ideal case are quantified by the continuous INLs as shown in Fig. 3(c), where the peak-to-peak INL (INL_{PP}) of the Hybrid-MRM transfer curve shows 2.65-bit (= 16.0-dB = ΔINL_{PP}) improvement over the NF-MRM transfer curve. The dynamic linearity for the analog E/O conversions is evaluated by the IMDs in the IP_3 measurements with a 5-GHz analog RF signal at V_P. As shown in Fig 3(d), the IMD of the Hybrid-MRMs exhibits 9.03-dB (= ΔIMD) improvement over the IMD of the NF-MRM, i.e., $\Delta SFDR_{IMD}$ = 3.01 dB. Also, the dynamic linearity for the digital E/O conversions is evaluated by the differential nonlinearity (DNL) and INL of the optical eye diagrams with 40-Gb/s PAM-8 random data at V_P. As shown in Fig. 3(e) and 3(f), the DNL_{PP} and INL_{PP} of the Hybrid-MRMs eye perform 2.02-bit (= 12.2-dB = ΔDNL_{PP}) and 2.15-bit (= 12.9-dB = ΔINL_{PP}) improvements, respectively, over the NF-MRM eye, within the 4.8-dB ER FS of the PAM-8 signal.

An initial test chip of the linearity enhancement technique has been fabricated at UCSD's NANO-3 facility in 220-nm silicon-on-insulator (SOI) SiPh process technology for rapid experimental validations in the lab. Instead of MRMs, the

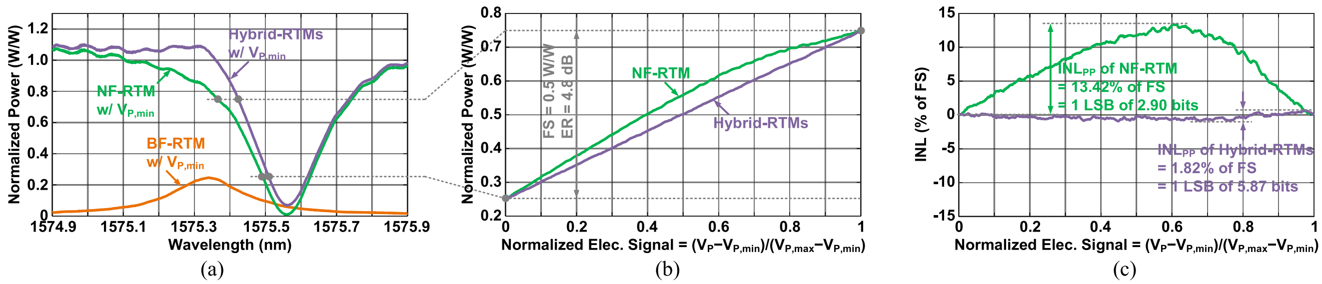

Fig. 5. The rapid experimental results using C-band passive RTMs fabricated at UCSD's NANO-3 facility: (a) The normalized power responses of the NF-RTM, BF-RTM, and Hybrid-RTMs when $V_P = V_{P,min}$. (b) The static E/O-conversion transfer curves of the NF-RTM and Hybrid-RTMs. (c) The INLs of the static E/O-conversion transfer curves in (b).

notch and bandpass filters are implemented by racetrack modulators (RTM), as shown in the chip photo of Fig. 4, which can offer better flexibility in designing the coupling coefficients and peaking behaviors of the resonators without affecting the whole concept of the linearity enhancement. Though this rapid fabrication can only produce the passive RTMs, the test chip can sufficiently demonstrate the power responses, static E/O-conversion transfer curves, and measurable INLs for proof of concept, as shown in Fig. 5, with Santec TSL-550 tunable laser sources, Newport 918D-IR-OD3R photodetectors (PD), and digitized data alignments. Under the predefined 4.8-dB ER FS, the INL_{PP} of the Hybrid-RTM transfer curve shows nearly 3-bit ($\approx$ 17.9-dB = ΔINL_{PP}) static-linearity improvement over the NF-RTM transfer curve.

IV. Discussions and Future Work

The summation process of P_{thru} and P_{drop} in Fig. 1(a) is done by the intensity detections of a dual-input PD during the O/E conversion at the far-end receiver (RX) side to generate the photocurrent $I_{PD} = (I_{thru} + I_{drop})$, which is linearly proportional to $(P_{thru} + P_{drop})$ based on the PD responsivity in the unit of A/W, and the following trans-impedance amplifier (TIA) linearly converts $(I_{thru} + I_{drop})$ to $(V_{thru} + V_{drop})$. In reality, not only the non-idealities of PD and TIA could further degrade the overall linearity, but also the latency mismatch between the two fibers could cause the propagation time deltas between $P_{thru}(t)$ and $P_{drop}(t)$, which is the primary concern of this linearity enhancement technique. For the example of a 5-GHz RF signal at V_P, a 20-ps latency mismatch between two 10-km long fibers can induce a certain amount of distortion when the $I_{thru}(t)$ and $I_{drop}(t)$ waveforms are summed in the time domain with a 10% (= 20-ps/200-ps) phase error. The Hybrid-MRM TX shown in Fig. 1(b) can resolve this issue by having a single fiber and two laser injections with well-spaced wavelengths so that $P_{thru}(t)$ and $P_{drop}(t)$ carried by λ_1-laser and λ_2-laser, respectively, can be coupled to a single fiber at the TX side to maintain an identical fiber latency without interfering with each other. This single-fiber Hybrid-MRM TX still satisfies the analysis shown in Fig. 2, but its P_{thru}/P_{in} and P_{drop}/P_{in} responses shall have an extra static wavelength offset because of the delta between λ_1 and λ_2, but the linearity enhancement concept remains valid since the linear power-envelope summation happens in the time domain, not in the frequency domain.

Due to various noise floors and sustainable optical power levels of all different photonic materials and electronic circuit operation environments, this letter can meaningfully report the improvement of $SFDR_{IMD}$, i.e., $\Delta SFDR_{IMD} = 3.01$ dB. If the noise floor is −169 dBm/Hz based on [9], and the TIA output power FS is −26 dBm, then the IP_3 in Fig. 3(d) is at (16.8 dBFS, −14.7 dBm), so the $SFDR_{IMD}$ of the Hybrid-MRMs is 103 dB. Eventually, the Hybrid-MRM TX, including all the electronic circuits and MRMs with segmented PN-junctions and thermal control capabilities, will be monolithically integrated and fabricated in GF45SPCLO to demonstrate an energy/area-efficient E/O interface with a high degree of linearity for various analog and digital optical communication systems.

References

[1] C. H. Cox et al., "Limits on the performance of RF-over-fiber links and their impact on device design," *IEEE Trans. Microw. Theory Techn.*, vol. 54, no. 2, pp. 906–920, Feb. 2006.

[2] C. Middleton et al., "Integrated optical beamformers," in *Proc. IEEE Avionics Vehicle Fiber-Optics Photon. Conf.*, Mar. 2015, pp. 61–62.

[3] C. Wang et al., "Integrated lithium niobate electro-optic modulators operating at CMOS-compatible voltages," *Nature*, vol. 562, no. 7725, pp. 101–104, 2018.

[4] J. Cardenas et al., "Linearized silicon modulator based on a ring assisted Mach Zehnder inteferometer," *Opt. Exp.*, vol. 21, no. 19, pp. 22549–22557, Sep. 2013.

[5] P. A. Morton et al., "High-power, high-linearity, heterogeneously integrated III–V on Si MZI modulators for RF photonics systems," *IEEE Photon. J.*, vol. 11, no. 2, pp. 1–10, Apr. 2019.

[6] M. Rakowski et al., "45 nm CMOS—Silicon photonics monolithic technology (45CLO) for next-generation, low power and high speed optical interconnects," in *Proc. Opt. Fiber Commun. Conf. Exhib. (OFC)*, San Diego, CA, USA, Mar. 2020, pp. 1–3.

[7] T. Baehr-Jones et al., "Monolithically integrated 112 Gbps PAM4 optical transmitter and receiver in a 45 nm CMOS-silicon photonics process," *Opt. Exp.*, vol. 31, no. 15, pp. 24926–24938, Jan. 2023.

[8] H. Li et al., "A 3-D-integrated silicon photonic microring-based 112-Gb/s PAM-4 transmitter with nonlinear equalization and thermal control," *IEEE J. Solid-State Circuits*, vol. 56, no. 1, pp. 19–29, Jan. 2021.

[9] A. Ayazi et al., "Linearity of silicon ring modulators for analog optical links," *Opt. Exp.*, vol. 20, no. 12, pp. 13115–13122, Jun. 2012.

[10] Y. Yuan et al., "A 100 Gb/s PAM4 two-segment silicon microring resonator modulator using a standard foundry process," *ACS Photon.*, vol. 9, no. 4, pp. 1165–1171, Apr. 2022.

[11] Q. Zhang et al., "Improving the linearity of silicon ring modulators by manipulating the photon dynamics," *IEEE Photon. J.*, vol. 12, no. 2, pp. 1–10, Apr. 2020.

[12] L. Chen et al., "Highly linear ring modulator from hybrid silicon and lithium niobate," *Opt. Exp.*, vol. 23, no. 10, pp. 13255–13264, May 2015.